Marine Pollution Bulletin 169 (2021) 112587

Contents lists available at ScienceDirect

Marine Pollution Bulletin

journal homepage: www.elsevier.com/locate/marpolbul

The transport, effective half-lives and age distributions of radioactive releases in the northern Indian Ocean

R. Periáñez [a,*], B.I. Min [b], K.S. Suh [b]

[a] Dpt Física Aplicada I, ETSIA, Universidad de Sevilla, Ctra Utrera km 1, 41013 Sevilla, Spain
[b] Korea Atomic Research Institute, Daedeok-Daero 989-111, Yuseong-Gu, Daejeon, Republic of Korea

ARTICLE INFO

Keywords:
Indian Ocean
Radionuclide
Sediment
Transport
Model

ABSTRACT

A Lagrangian model which describes radionuclide transport in the northern Indian Ocean is described. Water circulation is obtained from HYCOM ocean model for year 2017. The model includes advection by currents, turbulent mixing and radionuclide interactions between water and sediments, described in a dynamic way using kinetic transfer coefficients. Hypothetical releases from five coastal nuclear power plants operating in the northern Indian Ocean were simulated. Releases were supposed to start both during the winter and summer monsoons, to study reversing circulation effects. Age distributions of releases were calculated, which adds information about circulation and radionuclide pathways. It was found that, for some of the NPPs, radionuclide distributions resulting from releases starting in both seasons were not as different as could be expected from the opposed circulation schemes during each monsoon. Effective ^{137}Cs half-lives in the ocean surface were calculated and results were two orders of magnitude below previous estimations.

1. Introduction

The interest in improving models which simulate the behaviour and transport of radioactive elements in the marine environment increased since the Fukushima Dai-ichi Nuclear Power Plant (NPP) accident in 2011 in Japan, after which significant amounts of radionuclides were introduced into the Pacific Ocean directly from the NPP as well as deposited from the atmospheric releases resulting from hydrogen explosions in the NPP (Kobayashi et al., 2013). Such interest was embodied, for instance, in modelling programs launched by the International Atomic Energy Agency (IAEA): models were applied and compared in several release scenarios, not only to Fukushima releases into the Pacific (IAEA, 2019; Periáñez et al., 2016, 2019a, 2019b).

The northern Indian Ocean is a unique ocean since it is affected by monsoons and thus large scale circulation is seasonal. Essentially, during winter in the northern hemisphere a high pressure system is formed in central Asia, which results in northeast winds over the ocean. This is the winter (or northeast) monsoon. This high pressure system weakens and in summer a low pressure system of thermal origin results, which reverses wind directions. This is the summer (or southwest) monsoon. The winter monsoon extends from November to February and the summer one from May to September. The remaining months are transition ones from one monsoon to the other. Such atmospheric forcing affects circulation in the Indian Ocean, which is analyzed in detail in, for instance, Schott and McCreary (2001) and Shankar et al. (2002). A brief description of circulation in the northern ocean is given later.

Only two local-scale pollutant transport models for the northern Indian Ocean could be found in literature. A Lagrangian model was used to simulate tar ball transport in Goa coast in west India (Suneel et al., 2013). Patgaonkar et al. (2012) applied MIKE21 model to estimate the residence time of a small bay in northwest India. The transport of microplastics in the southern Indian Ocean was analyzed by Collins and Hermes (2019) using a Lagrangian model.

Several NPPs are operating along the shores (or close to) of the northern Indian Ocean. They are Kanupp NPP in Pakistan and Kakparar, Tarapar, Kaiga, Kudankulam and PFBR NPPs in India (see map in Fig. 1); actually, Kakparar and Kaiga are located some tens of km inland, but by rivers which discharge in the nearby coast. However, models which could be applied to simulate the oceanic dispersion of radionuclides released due to a potential accident occurring in any of the NPPs could not be found in literature. Fukushima accident in Japan showed us the need of having radionuclide marine transport models prepared to operate in areas which could be affected by a potential nuclear accident (IAEA, 2019; Periáñez et al., 2016). The purpose of the present paper

* Corresponding author.
E-mail address: rperianez@us.es (R. Periáñez).

https://doi.org/10.1016/j.marpolbul.2021.112587
Received 15 April 2021; Received in revised form 26 May 2021; Accepted 27 May 2021
Available online 7 June 2021

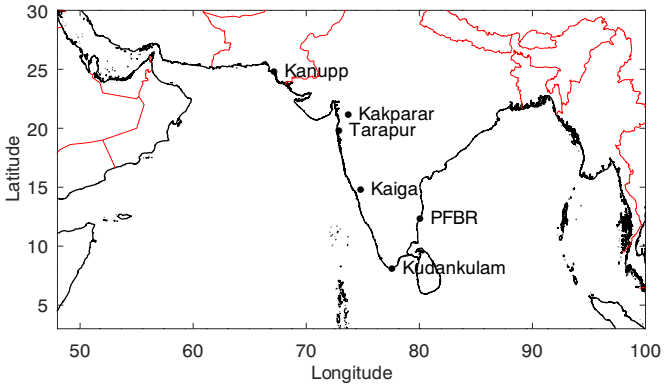

Fig. 1. Map of the Indian Ocean, corresponding to the model domain, showing the locations of coastal NPPs operating in the area.

consists of filling this gap and describing a radionuclide transport model for the northern Indian Ocean. This model could be used to simulate radionuclide transport from a hypothetical accident, as was done in the case of Fukushima accident, but also can provide insight into dispersion patterns resulting from different release scenarios (different release location and season). Different diffusion schemes were tested and results compared. Age distributions of the released particles were also provided by the model and effective half-lives of radionuclides in the northern ocean were calculated as well and compared with previous estimations. Thus, the present model is not only a tool which may help to assess the aftermath of a nuclear accident, but it can also be used in a more process-orientated investigation of the ocean.

Essentially, the model is a three-dimensional Lagrangian transport model forced with water circulation obtained from HYCOM (Bleck, 2001) global ocean model. The model includes physical transport (advection due to currents and mixing due to turbulence), uptake/release reactions between dissolved radionuclides and bed sediments, which are described in a dynamic way, and radioactive decay. It should also be commented that this model could be applied to other chemical pollutants (for instance heavy metals, ammonia etc.) simply setting radioactive decay to zero.

The model is briefly described in Section 2. Results of the different numerical experiments are presented and discussed in Section 3. First, a brief description of circulation in the northern Indian Ocean is included in Section 3.1, then radionuclide simulations are presented in Section 3.2. Within this section, the radionuclide releases are described in Section 3.2.1, turbulence models are compared in Section 3.2.2, radionuclide transport simulations from the different NPPs and calculation of half-lives are described in Section 3.2.3 and, finally, age distributions are discussed in Section 3.2.4. Main conclusions are summarized in Section 4.

2. Model description

2.1. Baroclinic circulation

HYCOM (Hybrid Coordinate Ocean Model [Bleck, 2001]) model was used to obtain circulation in the Indian Ocean. HYCOM is a primitive equation general circulation model with horizontal resolution equal to $\Delta x = \Delta y = 0.08^\circ$ and 40 vertical layers. The model web page (https://www.hycom.org/) provides examples of applications over the world, as well as a detailed description of the model. In particular, HYCOM model is forced by winds, short and long wave radiation and freshwater inflow through the main rivers. The system uses the Navy Coupled Ocean Data Assimilation (NCODA) system (Cummings, 2005; Cummings and Smedstad, 2013).

Daily currents of year 2017 were downloaded from HYCOM data server. This year was selected because there are not missing data for it in HYCOM data server and, also, any anomalous circulation feature was not observed in the northern ocean, thus it can be considered as a typical year. Nevertheless, it is worth to comment that an Indian Ocean Dipole (IOD) was observed in 2017 (Zhang et al., 2018). It mainly affects the southern hemisphere and consists of an ocean-atmosphere coupled mode in the tropical Indian Ocean which features a sea surface temperature anomaly gradient. This anomaly is quantified by the dipole mode index, the difference of area-averaged sea surface temperature anomaly between the western tropical ocean (50°-70°E, 10°N-10°S) and the southeastern tropical Indian Ocean (90°-110°E, Equator-10°S). During a positive IOD index period anomalous easterly winds prevail along the equator and leads to severe flood in East Africa and drought in the Indonesian Archipelago (Zhang et al., 2020). However, after analyzing currents in the northern Indian Ocean (which is the domain of the model) in 2017, any significant effect of this IOD event could not be observed.

2.2. Radionuclide transport model

As mentioned before, the model is Lagrangian or particle-tracking. The radionuclide release is thus simulated by means of a number of particles. Each particle is equivalent to a number of units (for instance Bq) whose trajectories are evaluated during the simulated time period. Transport processes are physical advection due to water currents and mixing due to turbulence. In addition, the model includes radioactive decay and interactions of radionuclides with bed sediments (adsorption/desorption reactions). Radionuclide concentrations are evaluated from the number of particles within each grid cell and compartment (surface water, deep water and sediment).

In a Lagrangian model advection is obtained from the following equation for each particle:

$$L_x = u\Delta t + \frac{\partial K_h}{\partial x}\Delta t \quad (1)$$

$$L_y = v\Delta t + \frac{\partial K_h}{\partial y}\Delta t \quad (2)$$

where L_x and L_y are the changes in particle position; u and v are water velocity components at the particle position and depth and for the corresponding calculation time step, since currents change in time, downloaded from HYCOM model. Note that daily HYCOM currents are used.

Derivatives of the horizontal diffusion coefficient (K_h) prevent the artificial accumulation of particles in regions were diffusion coefficients are smaller (Proehl et al., 2005).

A first order accuracy scheme was applied to solve advection. However, Elliott and Clarke (1998) did not find improvements in results if a second order accuracy scheme were used. Moreover, turbulence masks small errors in the advection scheme (Elliott and Clarke, 1998).

The maximum size of the horizontal step given by the particle due to turbulent mixing, D_h, is (Proctor et al., 1994; Periáñez and Elliott, 2002):

$$D_h = \sqrt{12K_h\Delta t} \quad (3)$$

in the direction $\theta = 2\pi RAN$, where RAN is a uniform random number between 0 and 1 and Δt is time step in the Lagrangian model. This equation gives the maximum size of the step. The real size at a given time and for a given particle is obtained multiplying the equation by another independent random number. This procedure is required to ensure that a Fickian diffusion process (Proctor et al., 1994) is simulated. Time step used to integrate the Lagrangian model was set as $\Delta t =$ 600 s.

Similarly, the size of the vertical step is (Proctor et al., 1994; Periáñez and Elliott, 2002):

$$D_v = \sqrt{2K_v\Delta t} \quad (4)$$

given either upward or downward. In this equation K_v is the vertical diffusion coefficient.

Three different schemes were tested to describe turbulent mixing. The simplest model, denoted as UD (uniform diffusivities) uses uniform and constant values for K_h and K_v. Model denoted as SD uses a Smagorinsky scheme (Cushman-Roisin and Beckers, 2011) for K_h and constant and uniform K_v. Finally model SDV uses the Smagorinsky scheme for K_h and K_v is described as a function of depth, although remaining constant in time.

In case of the UD model, horizontal and vertical diffusivities are respectively set as 10 m^2/s (Periáñez, 2020) and 1.0×10^{-5} m^2/s (Elliott et al., 2001; Brovchenko and Maderich, 2021). This same value is used for K_v in the SD model.

The Smagorinsky scheme (Cushman-Roisin and Beckers, 2011) used in SD and SDV models describes the horizontal diffusion coefficient as a function of the grid spacing, Δx and Δy, and the horizontal shear of currents:

$$K_h = \Delta x \Delta y \sqrt{\left(\frac{\partial u}{\partial x}\right)^2 + \left(\frac{\partial v}{\partial y}\right)^2 + \frac{1}{2}\left(\frac{\partial u}{\partial y} + \frac{\partial v}{\partial x}\right)^2} \quad (5)$$

Finally, vertical diffusion in the SDV model is written following the description in Periáñez et al. (2019b) used to describe radionuclide transport in the Pacific Ocean after Fukushima accident:

Table 1
Parameters used in the radionuclide transport model.

Parameter	Description	Value
ρ_m	Mineral particle density	2600 kg/m^3
por	Sediment porosity	0.6
ϕ	Sediment correction factor	0.1
k_2	Desorption rate	1.16×10^{-5} s^{-1}
d_{pic}	Surface layer thickness	100 m

$$K_v = \begin{cases} 10^{-3} \ m^2/s & z < 60 \ m \\ 10^{-5} \ m^2/s & z > 120 \ m \\ \text{lineal function} & 60 < z < 120 \ m \end{cases} \quad (6)$$

where z is water depth below the sea surface. This way increased turbulence in the mixed layer of the ocean is described, while it is smaller in the pycnocline and deep ocean. Using a constant mixed layer thickness is just an approximation to speed up calculations; of course this thickness is seasonally variable and its climatological mean ranges from some 30 to 100 m in the Indian Ocean (Schiller and Oke, 2015). The Smagorinsky scheme is used in this model as mentioned before.

Of course, these mixing schemes are approximations focused at achieving the short simulation times required in nuclear emergency models. Actually, they were applied in the most recent radionuclide transport models used in the International Atomic Energy Agency (IAEA, 2019) to simulate Fukushima NPP releases in the Pacific Ocean. A review on more sophisticated models can be seen in Davies et al. (1997a,

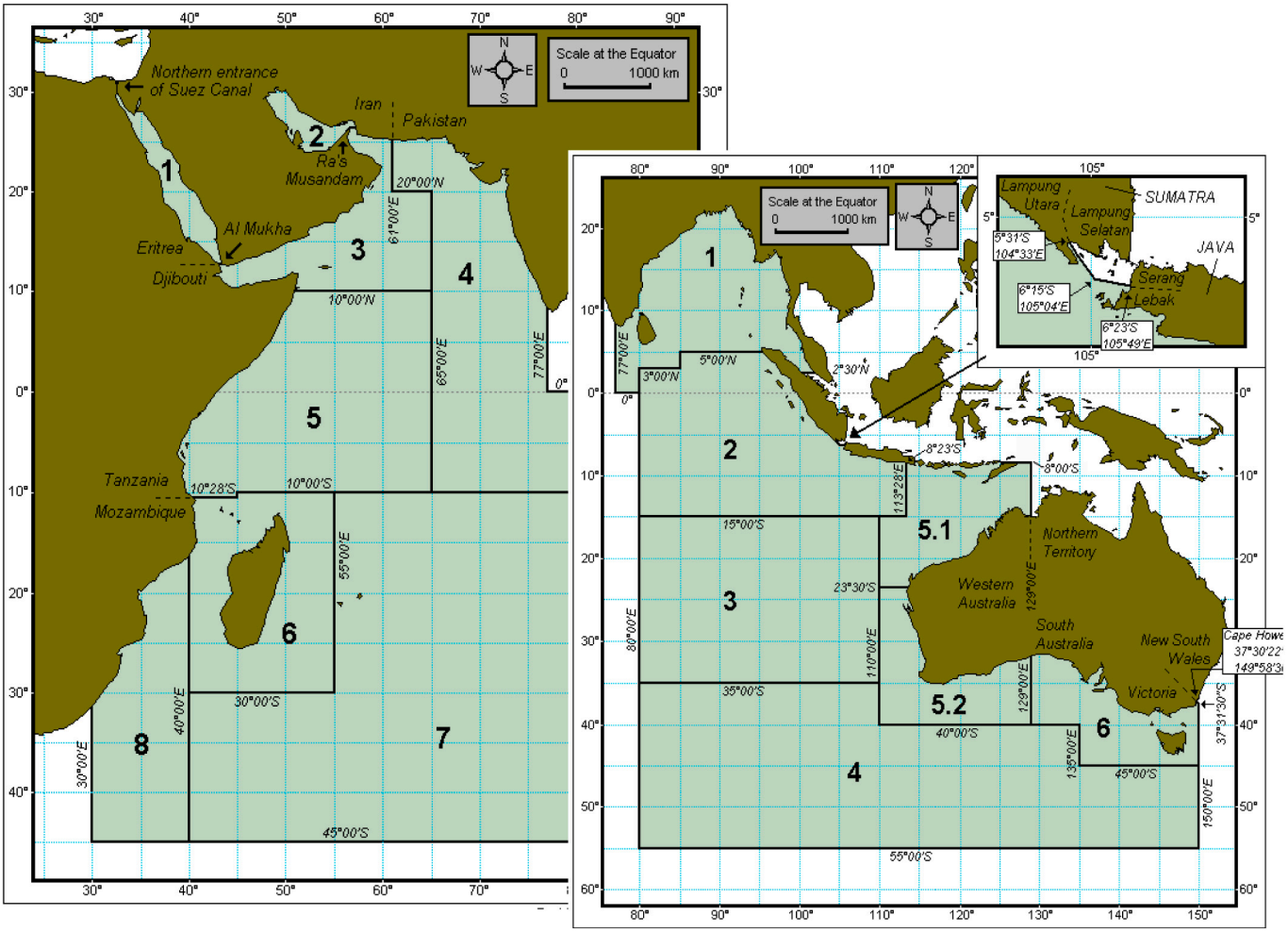

Fig. 2. Map of the Indian Ocean showing its division into FAO major fishing areas.
Source: http://www.fao.org/fishery/area/search/en.

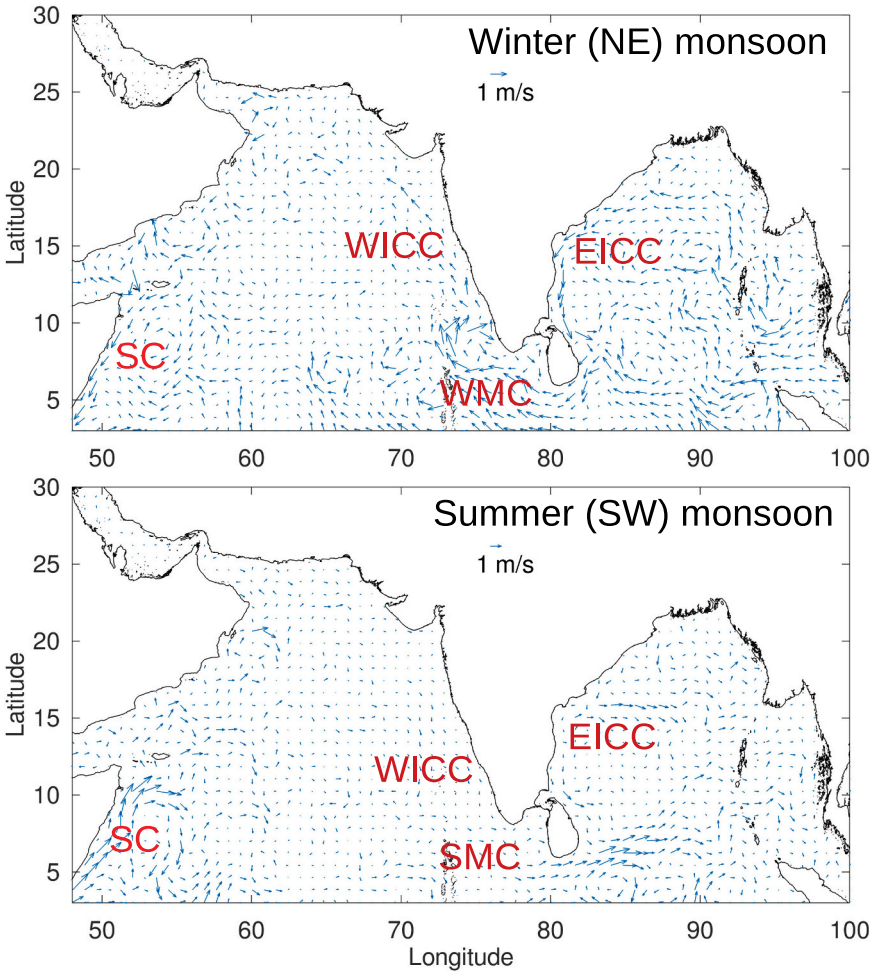

Fig. 3. Surface currents in the northern Indian Ocean, as downloaded from HYCOM data server, for summer (or SW) and winter (or NE) monsoons. Snapshots of surface currents corresponding to year 2017 for December 31th (winter) and August 1st (summer) are drawn. SC: Somali Current, WICC: West India Coastal Current, EICC: East India Coastal Current, WMC: Winter Monsoon Current, SMC: Summer Monsoon current. Only one of each 100 current vectors is drawn for more clarity.

1997b).

Radioactive decay is solved with a stochastic method (Periáñez and Elliott, 2002). Decay probability is defined as:

$$p_d = 1 - e^{-\lambda \Delta t} \tag{7}$$

where λ is the radioactive decay constant. A new random number is generated. If $RAN \leq p_d$ the particle is considered to decay and it is removed from the computation.

The interactions of radionuclides between water and the bed sediments are described in terms of a kinetic adsorption rate k_1 and a desorption rate k_2; and a stochastic method is applied as well. The probability that a dissolved particle is adsorbed by the sediment is:

$$p_a = 1 - e^{-k_1 \Delta t} \tag{8}$$

If a new generated independent random number is $RAN \leq p_a$, then the particle is fixed to the sediment. The probability that a particle which is attached to the sediment is released to water is:

$$p_r = 1 - e^{-k_2 \phi \Delta t} \tag{9}$$

and the same procedure is used. ϕ is a correction factor that takes into account that part of the surface of sediments is hidden by the surrounding sediments. Thus, this hidden part is not interacting with the water.

The number of units (in this case Bq) corresponding to each particle, R is deduced from the number of particles used in the simulation (NP = 200, 000) and the magnitude of the release M (total released activity):

$$R = \frac{M}{NP} \tag{10}$$

Then radionuclide concentration in the water surface layer of each grid cell $C_{surf}(i,j)$ (in Bq/m^3) is:

$$C_{surf}(i,j) = \frac{RN_{surf}(i,j)}{\Delta x \Delta y d_{pic}} \tag{11}$$

where $\Delta x \Delta y$ is the cell surface, $N_{surf}(i,j)$ is the number of particles within the surface layer in cell (i,j) and d_{pic} is the surface layer thickness (thus we count only particles at depth less than d_{pic}). The radionuclide inventory (Bq/m^2) in water below the surface layer (from d_{pic} to the seabed) is given by:

$$I_{deep} = \frac{RN_{deep}(i,j)}{\Delta x \Delta y} \tag{12}$$

where $N_{deep}(i,j)$ is the number of particles in cell (i,j) at depth larger than d_{pic}. Finally, bed sediment radionuclide concentration (Bq/kg) in cell (i,j) is:

$$C_{sed}(i,j) = \frac{RN_{sed}(i,j)}{\Delta x \Delta y L \rho_s} \tag{13}$$

where $N_{sed}(i,j)$ is the number of particles in the bed sediment of cell (i,j), L is sediment thickness (set as 0.05 m) and ρ_s is sediment bulk density:

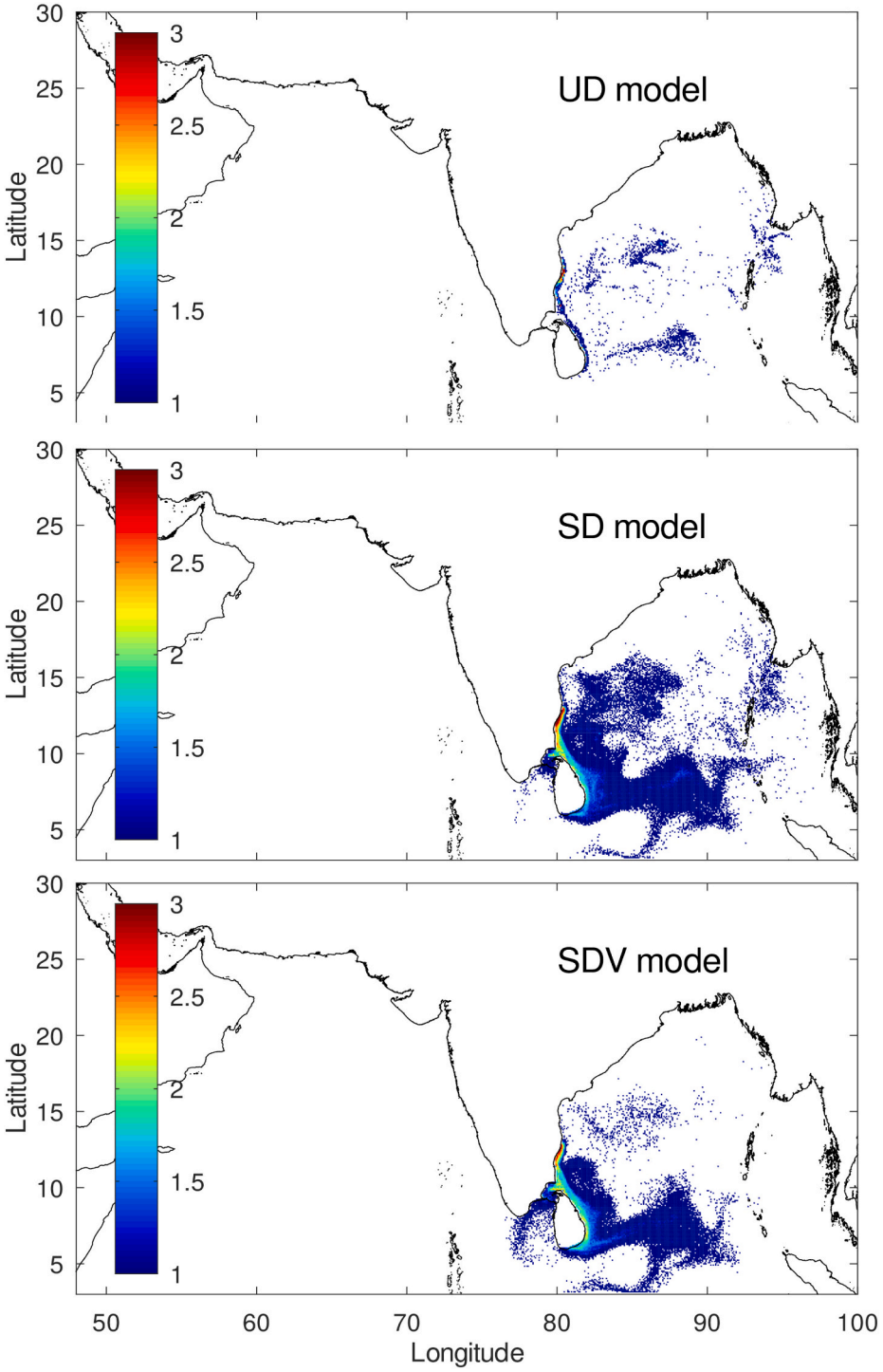

Fig. 4. Calculated water surface ^{137}Cs concentrations (Bq/m^3) in logarithmic scale with the three turbulent mixing models. These simulations correspond to the PBFR NPP summer accident.

$$\rho_s = \rho_m(1 - por) \tag{14}$$

where ρ_m is mineral particle density and *por* is sediment porosity. A number of parameters are defined within the model code, whose values are selected from standard ones or previous works. These parameters are summarized in Table 1. The adsorption rate k_1 is deduced from the desorption rate k_2 and the radionuclide distribution (or partition) coefficient k_d for ocean waters, which can be obtained from IAEA (2004), following the procedure described in Periáñez (2008) for instance. The desorption rate k_2 was obtained from the experiments in Nyffeler et al. (1984), value which was used in many other modelling works (see for instance Periañez et al., 2013 and the review in Periáñez et al., 2019a).

In addition, ages of particles in the ocean were calculated. The age is defined as the time elapsed since a given particle was released into the sea, and may provide useful information about circulation in a marine region. It is a Lagrangian concept and is obtained simply attaching a clock to each particle, which is started in the moment when the particle is released. The age-averaging hypothesis, as introduced by Deleersnijder et al. (2001), was used: the mean age of particles which are within each grid cell is defined as the mass-weighted arithmetic average

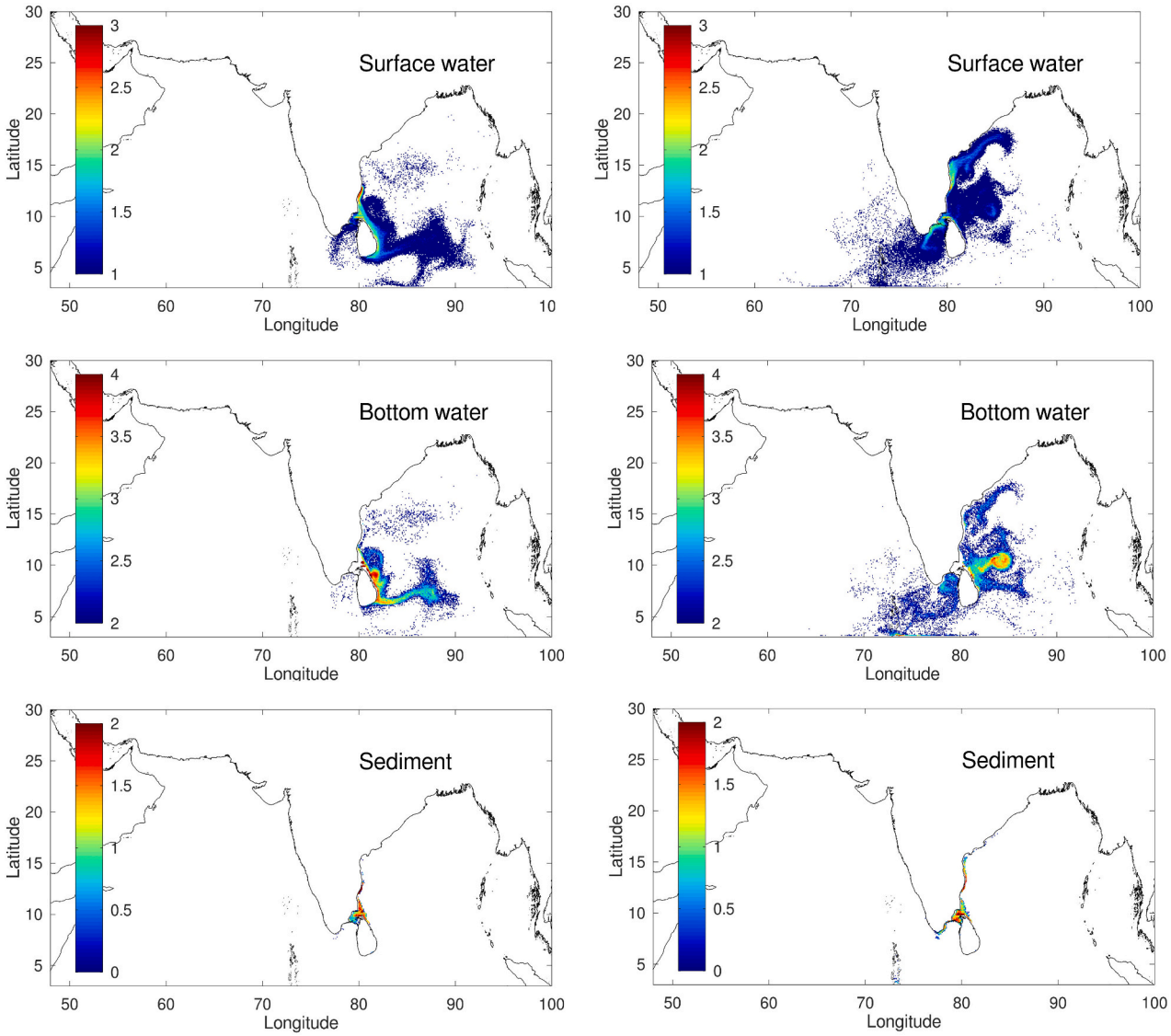

Fig. 5. Calculated ^{137}Cs concentrations in the surface water layer (Bq/m^3), inventory in the deep layer (Bq/m^2) and concentrations in bed sediments (Bq/kg) for releases occurring during the summer (left column) and winter (right column) monsoons from PFBR NPP. Logarithmic scales are used.

of the ages of the particles present there. The mass of particle *i* is defined as its radioactivity content R_i, thus the mean age, $\langle age \rangle$, in a given grid cell is:

$$\langle age \rangle = \frac{\sum_{i=1}^{N} \tau_i R_i}{\sum_{i=1}^{N} R_i} \tag{15}$$

where N is the number of particles within the cell and τ_i is the reading of the clock attached to particle *i*. If the values of R_i were the same for all particles, then the mean age is the arithmetic means of the clock readings:

$$\langle age \rangle = \frac{1}{N} \sum_{i=1}^{N} \tau_i \quad \text{if} \quad R_i = R \quad \forall i \tag{16}$$

The temporal evolution of the average radionuclide concentrations in the surface layer over several areas of the northern Indian Ocean are finally calculated to assess the potential effect of a given release in fishery areas defined by FAO (Food and Agricultural Organization of the United Nations). These areas are shown in Fig. 2. We consider region 1 (Bay of Bengal) in the eastern ocean, and the western ocean is divided into regions 3 (western Arabian Sea), 4 (eastern Arabian Sea) and the part of region 5 (Somalia) which is within the model domain (northern portion of this region). The marginal Red Sea and Arabian/Persian Gulf are not considered.

Of course these averages over such large regions cannot be used to evaluate the impact of NPP accidents on fisheries during the acute phase of the accident, since very high concentrations are locally produced in the region close to the NPP and negligible values far from it. However, they can provide information on the general trends of radionuclide distributions at longer temporal scales, when a relatively high homogenization of the radionuclide patch can be expected. Actually, this methodology consisting of dividing the ocean space into relatively large boxes was recently used in Periáñez et al. (2019b) to study the impact of Fukushima NPP accident in the Pacific Ocean and to compare model predictions with measurements. In addition, these calculations allow the calculation of ^{137}Cs effective half-lives for such areas of the Indian Ocean. Some estimations of this figure were already provided by Povinec et al. (2005) and Sartandel et al. (2015). These authors consider that the average ^{137}Cs concentration in the ocean surface, *C*, appears to decrease exponentially with time and thus is described by the following equation:

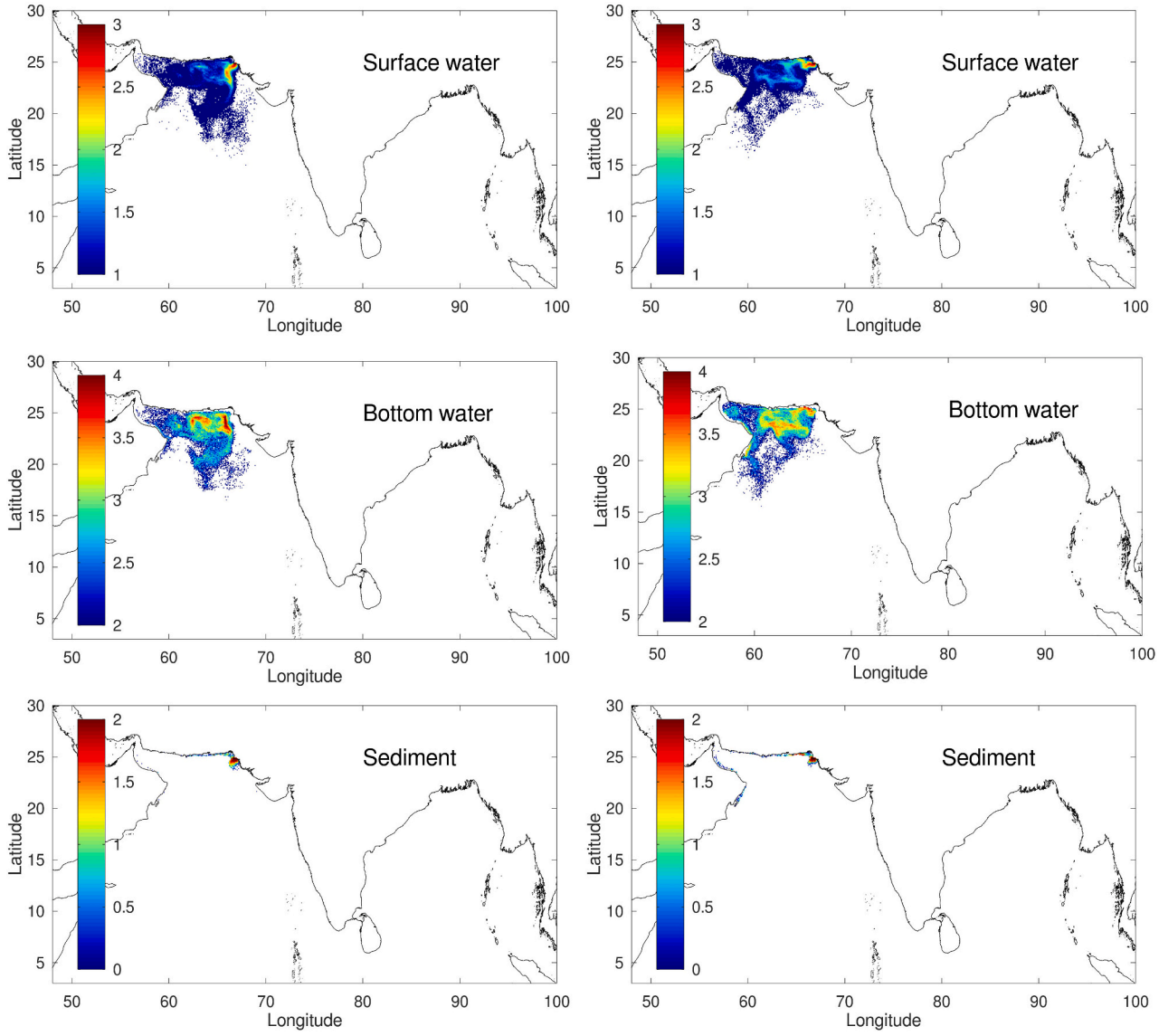

Fig. 6. Same as Fig. 5 but for releases occurring from Kanupp NPP.

$$\frac{dC}{dt} = -FC, \tag{17}$$

where F is a flux coefficient. The effective half-life is then:

$$T_{1/2} = \frac{ln2}{F}, \tag{18}$$

and is calculated fitting the temporal trend of the radionuclide concentration in the ocean surface to an exponential decay function.

3. Results and discussion

A brief description of water circulation in the northern Indian Ocean, based upon currents calculated by HYCOM model is given first. Next results of radionuclide transport simulations are presented.

3.1. Circulation in the northern Indian Ocean

Typical surface water circulation schemes for both monsoons are presented in Fig. 3, as downloaded from HYCOM data server. The summer monsoon map corresponds to August 1st and the winter monsoon map is obtained in December 31th. Note that daily currents are used in the radionuclide transport model, as explained before, and these maps are snapshots of surface circulation at the mentioned days, as examples. The names of the main currents are included in the maps. Essentially, it is well known that currents are seasonally reversing. Thus, in winter the overall current direction in the northern ocean is to the west: the East India Coastal Current (see Fig. 3) flows to the south, the Winter Monsoon Current to the west in the south of India and the West India Coastal Current to the north along the western India coast. Finally, the Somali Current flows to the south along the eastern Africa coast. The pattern reverses in summer, with the Somali Current flowing towards the north and a general current direction to the east. Circulation in the Arabian Sea is anticyclonic in summer and cyclonic in winter (see for instance Schott and McCreary, 2001). This circulation scheme is reproduced by HYCOM ocean model, as can be seen in Fig. 3.

It is interesting to point out that conditions for coastal upwelling in the Indian Ocean are different than those of the Atlantic and Pacific ones, where this process occurs along the eastern coasts. The strongest upwelling takes place in the Indian Ocean along Somalia and Arabia coasts, when the SW monsoon forcing produces Ekman transport away from such coasts (Tomczak and Godfrey, 2003).

A detailed description of physical oceanography of the Indian Ocean, which is not the purpose of the present paper, may be seen for instance

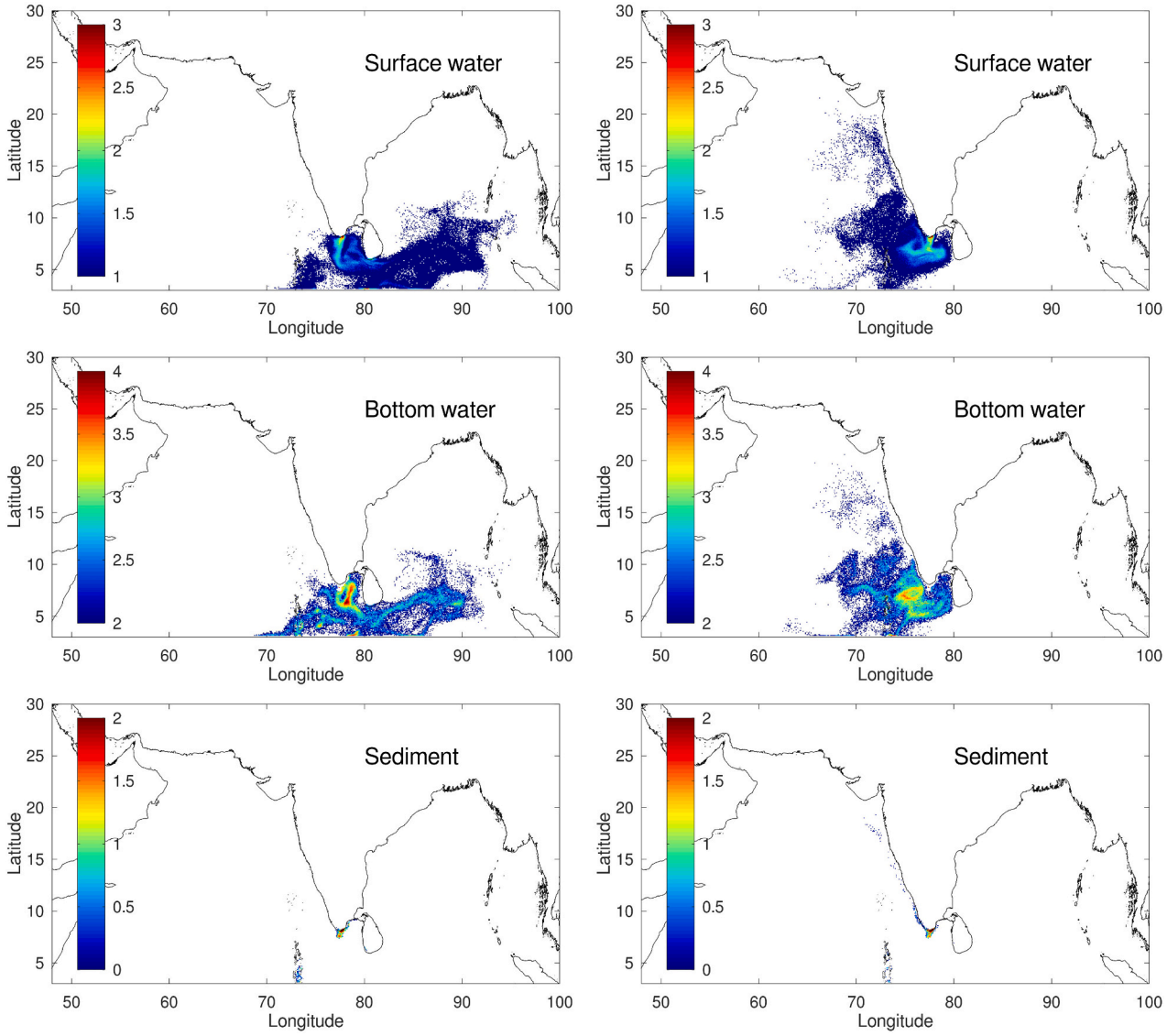

Fig. 7. Same as Fig. 5 but for releases occurring from Kudankulam NPP.

in Tomczak and Godfrey (2003), Shankar et al. (2002) and Schott and McCreary (2001).

3.2. Radionuclide transport

3.2.1. Radionuclide releases

A number of numerical experiments were carried out to assess the transport of radionuclides from the four coastal NPPs (see Fig. 1) and under winter and summer monsoon conditions. A ^{137}Cs (radioactive decay constant 7.31×10^{-10} s^{-1}) release of 1 PBq lasting 90 days (at a constant rate) was supposed to occur at the sea surface. This amount is an example of the same order of magnitude as the ^{137}Cs direct release from Fukushima into the Pacific Ocean in the first three months after the accident (Kobayashi et al., 2013). Thus, this figure is just an example to simulate a realistic accident. The ^{137}Cs distribution coefficient k_d was taken as 4.0 m^3/kg, which is the recommended value for coastal waters by IAEA (2004) for this radionuclide. The open ocean k_d (2.0 m^3/kg) was not used since water/sediment interactions occur in the shallow coastal areas. Simulations were 365 days long; the winter monsoon accidental release was supposed to start on December 15th and the summer monsoon release on May 15th.

3.2.2. Comparison of mixing models

First, results from the three mixing models were compared. A summer monsoon accident occurring in PFBR NPP was simulated using the UD, SD and SDV models. Resulting ^{137}Cs concentrations in the surface water layer after 90 days are presented in Fig. 4. The Smagorinsky scheme produces horizontal diffusivities larger than the 10 m^2/s defined in the UD model. Thus, in the SD and SDV models there is a higher offshore transport of radionuclides than in the UD model. This implies a higher fixation of radionuclides on the coastal seabed sediments in this model (result not shown) than with SD and SDV models. The SDV model uses a higher vertical diffusivity in the surface layer than the other two models. Thus, in this model transport of radionuclides to the deep water layer is higher than in UD and SD models. Consequently, surface water radionuclide concentrations in the central ocean are higher with SD than with SDV model (Fig. 4). In contrast, radionuclide content in the deep water layer is higher with the SDV model (result not shown).

Another significant difference between models is running time. For the 365 days long simulation, computation times on a desktop PC were respectively 32 min, 381 min and 397 min with the UD, SD and SDV models. The calculation of Smagorinsky diffusivities over the large computational domain and the 40 vertical levels is quite demanding.

If the purpose of a simulation is the rapid assessment of the effects of

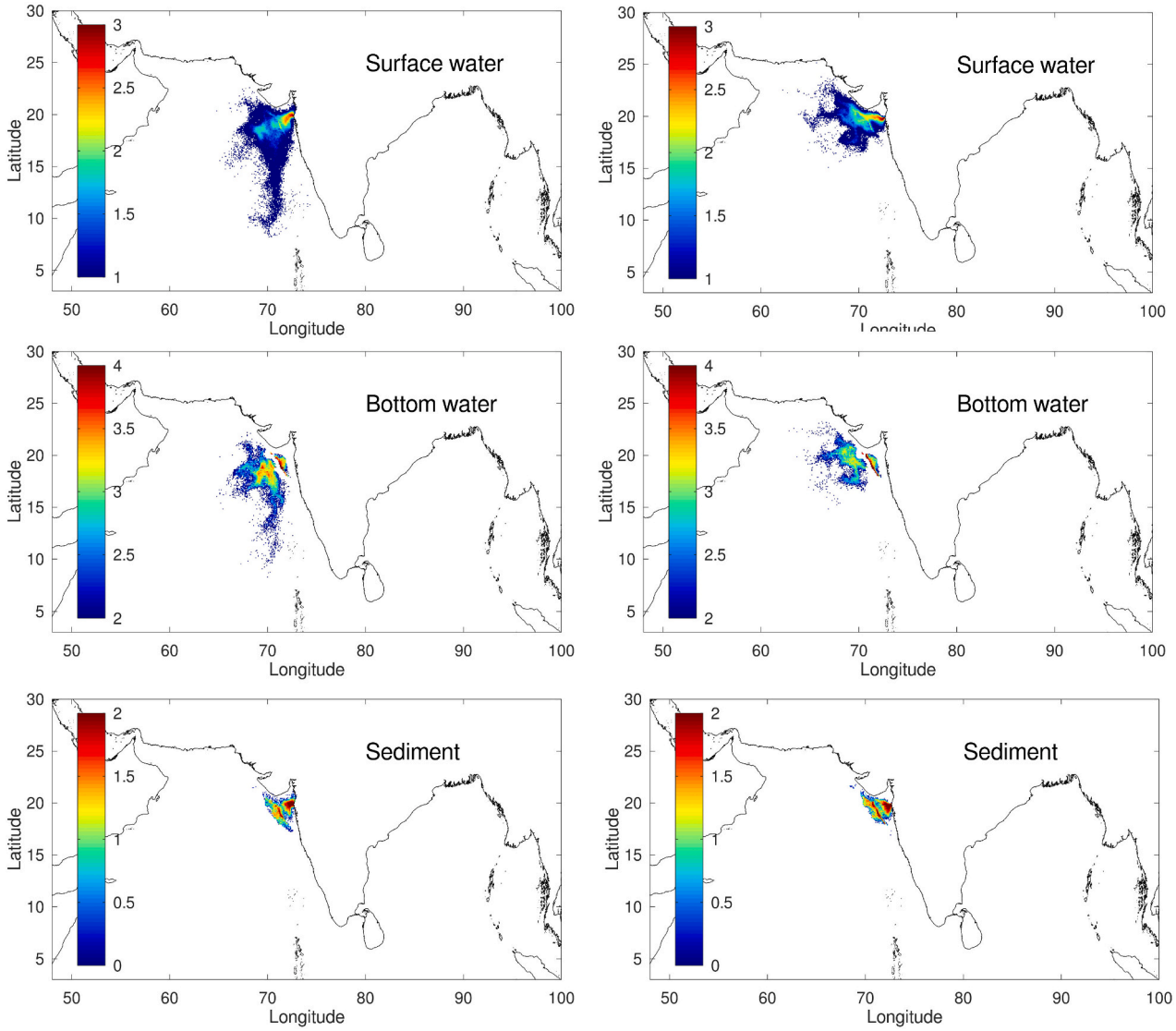

Fig. 8. Same as Fig. 5 but for releases occurring from Tarapur NPP.

an accident in the local area around the NPP, the UD model may be adequate: it provides a fast response and, due to the smaller diffusion coefficients, radionuclide concentrations in water and sediments over such local area tend to be overestimated, thus providing a conservative calculation (i.e., maximum possible values) which is a useful concept in radiological protection (IAEA, 2001). For a more refined evaluation, and also to assess transport over larger spatial scales, the SDV model is recommended. Note that a fast simulation would not be a requirement for such a large scale evaluation.

3.2.3. *Radionuclide transport from the NPPs*

As mentioned in Section 3.2.1 two simulations were carried out for each coastal NPP, for summer and winter monsoons, lasting 365 days. Calculated ^{137}Cs concentrations in the water surface layer, inventory in the deep layer and concentrations in the bed sediments can be seen in Figs. 5 to 8. These maps are obtained after 90 days, i.e., just at the moment when releases stop.

It can be first observed that, as a general result, contamination of the sediment is essentially limited to the coastal area close to the release point. Only in the case of Tarapur NPP releases (Fig. 8) a larger portion of seabed is affected by the release. Actually, this contamination extends to the border of the continental shelf, which is of the order of 100 km wide here, the widest in all the coast around Pakistan and India (it is similar only in the northern Bay of Bengal). The narrow continental shelf prevents the sediment contamination offshore.

The second result is that radionuclide distributions in water resulting from releases starting in summer and winter monsoons are in general not so different as could be initially expected from the different circulation schemes (shown in Fig. 3). They are particularly similar in the case of Kannup releases (Fig. 6), thus this region of the northern Arabian Sea seems to be little affected by the seasonally changing monsoon circulation. They are also not very different in the case of Tarapur NPP releases (Fig. 8), at least in the coastal region.

The most significant differences appear in the case of Kudankulam NPP releases (Fig. 7), in the most southern point of India. Currents are stronger in this region (Fig. 3) and radionuclides, once they reach the nearly flowing WMC or SMC, are efficiently transported to the west or east respectively. In the case of releases starting in summer, they are mainly transported to the central Bay of Bengal, while winter releases tend to flow northwards along the western India coast.

Releases from PFBR tend to travel to the central Bay of Bengal, however the east (west) coast of Sri Lanka is contaminated in case of summer (winter) monsoon releases (Fig. 5).

Generally speaking, the radionuclide distributions below the water surface layer are reproducing the situations in the surface. Thus, there is not a significant difference between the surface and deep circulation in

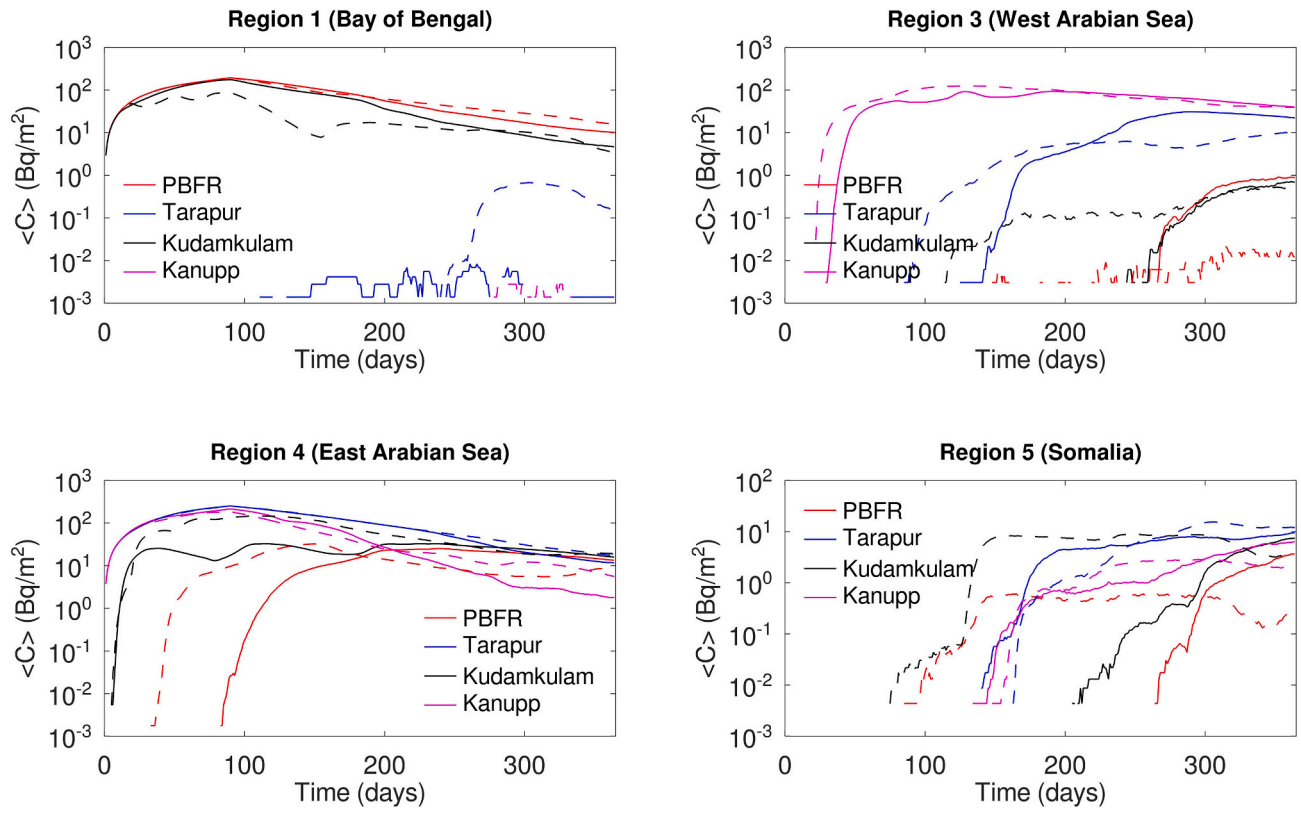

Fig. 9. Average concentrations per unit area calculated in the surface layer over the FAO fisheries. The dashed lines correspond to releases starting in winter monsoon and solid lines to releases starting in summer monsoon for each NPP.

Table 2
Effective half-lives in years calculated for each region surface layer. The fitting r^2 is given in parenthesis.

Region	Winter	Summer
1	0.15 (0.996)	0.19 (0.996)
3	0.38 (0.998)	1.7 (0.999)
4	0.21 (0.999)	0.23 (0.998)

the considered regions of the Indian Ocean. Nevertheless, as it will be commented below, most of the released radionuclides are introduced into the deep water layer.

Mean radionuclide concentrations in the surface layer in area 1 of the eastern ocean and areas 3, 4 and 5 of the western ocean (as defined by FAO and presented in Fig. 2) are shown in Fig. 9. They are calculated as the total activity in the surface layer divided by the area of the region, consequently they are given in Bq/m^2. If they are divided by the thickness of the surface layer (100 m in the present application, see Table 1), the radionuclide concentration in Bq/m^3 would be obtained. Povinec et al. (2005) estimated a mean ^{137}Cs concentration in the northern ocean surface of 1.5 Bq/m^3 in year 2000 and Sartandel et al. (2015) provided a value of 0.69 Bq/m^3 along Indian coasts in 2014. Taking into account that the considered surface layer thickness is d_{pic} = 100 m, background surface concentration per unit area in the northern ocean may be assumed to be in the order of 10^1 Bq/m^2.

Region 5, far from all NPPs, is not affected by the accidents, since concentrations remain similar or below background (Fig. 9). The other regions are obviously more affected by accidents occurring in NPPs located in or near their coasts, as PBFR and Kudankulam in region 1 and Kanupp in region 3. The oscillatory nature of currents produces that the east Arabian Sea (region 4) is affected by releases from all NPPs. In the case of this region, releases from PBFR arrive about 50 days earlier for the winter accident than for the summer one since winter circulation is directed to the west. Equivalent delays are observed in other regions. As commented before, concentrations may locally be orders of magnitude above background (see maps in Figs. 5–8), but these graphics may be useful to estimate the arrival time of a discharge to a given region of the ocean.

As explained in Section 2, effective half-lives of ^{137}Cs in the ocean surface were calculated from these temporal trends. They were calculated for each region using the NPP which is within it; thus PBFR was used for region 1, Kanupp for region 3 and Tarapur for region 4. The part of the each plot where concentrations decrease (i.e., from day 90 on, once releases stop) were fitted to an exponential decay curve and $T_{1/2}$ obtained from it. Results are presented in Table 2.

Half-lives range from about two months to two years and, with the exception of region 3, there is not any significant seasonal difference. These values are in general two orders of magnitude below those reported by Povinec et al. (2005) and Sartandel et al. (2015) for the whole northern ocean surface, which range 14–20 years. Actually, the half-life of the northern ocean as a whole was calculated as well from the temporal evolution of the average ^{137}Cs concentration over northern ocean surface, C_{ocean}, which is calculated using the following equation:

$$C_{ocean} = \frac{\sum_{i=1}^{4} A_i C_i}{\sum_{i=1}^{4} A_i} \tag{19}$$

where A_i is the surface of each of the four regions and C_i their mean ^{137}Cs concentrations. The resulting mean half-life of ^{137}Cs in the northern ocean from the 8 simulations (4 NPPs, two seasons) is 0.19 ± 0.02 y, where the error is the 1σ standard deviation of the mean.

The two orders of magnitude difference between our calculations and the previous estimations may be attributed to two reasons: a) Povinec et al. (2005) and Sartandel et al. (2015) apply Eq. (17) to real measurements of ^{137}Cs concentrations, without taking into account any external source of radionuclides to the ocean occurred since 1963

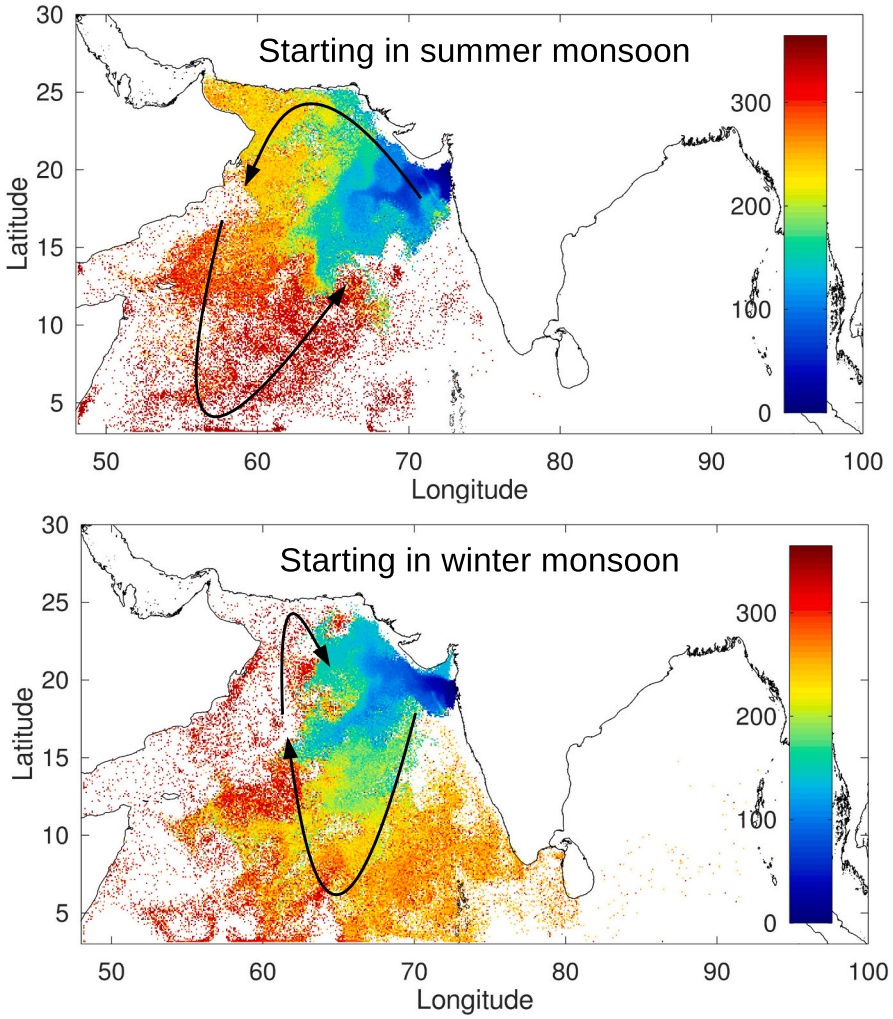

Fig. 10. Age distributions (days) in the surface layer for releases occurring from Tarapur NPP starting on May 15th and December 15th (top and bottom respectively).

(fallout, major accidents etc.). In other words, a source term should be added to the right hand side of Eq. (17). Therefore, it is not surprising that essentially the same effective half-life of ^{137}Cs is reported for the Indian, Atlantic and Pacific oceans, as well as for the global ocean, if they are calculated in this way (see Table 5 in Sartandel et al., 2015). Of course, our numerical experiments do not present this shortcoming. b) The number of measurements is extremely small, and they are extrapolated from local areas to be representative of the whole ocean. For instance, Sartandel et al. (2015) use measurements along India coast as a proxy for the whole northern Indian Ocean.

Calculated half-lives indicate a fast removal of ^{137}Cs from the ocean surface. Using the summer releases from PBFR as an example, it was found that at the end of the simulation (1 year of simulation with a 90 day discharge as already explained) only 0.79% of the released ^{137}Cs is fixed to the sediment while 94.6% of it is in the water phase. The remaining 4.61% has decayed or left the computational domain. Considering the amount remaining in water, 8.51% of it is in the surface layer and the remaining 91.5% is below it. Thus, mixing due to turbulence produces a fast migration of radionuclides to the deep ocean and leads to the short calculated effective half-lives in the ocean surface.

3.2.4. Age distributions

In order to calculate the age distributions due to NPP releases only three of them were considered: in the west India coast (Tarapur), south of India (Kudankulam) and east India coast (PFBR). In addition, the radionuclide k_d and radioactive decay constant λ were set to zero in these particular simulations. Thus, age distributions are only governed by hydrodynamic processes, since interactions with sediments and radioactive decay are switched off. In agreement with the previous section, age distributions in the surface and deep water layers are very similar, thus only results for the surface layer are presented.

The age distributions resulting from releases occurring in Tarapur NPP are presented in Fig. 10. Obviously the colored parts of the map indicate the extension of contamination, since age is zero in a given grid cell if there are not any particles there. These extensions are not very different, taking into account that releases started with a temporal difference of half a year. This result is confirming what was commented in Section 3.2.3. However, age distributions help to visualize the circulation of pollutants. Thus, if releases start with summer monsoon pollutant circulation tends to be cyclonic in the north-western Indian Ocean: age increases progressively from Tarapur NPP towards the northwest, then to the southwest along Africa coast and finally towards the northeast, with particles approaching the release point. This pattern is reversed to anticyclonic in the case of releases starting in winter monsoon: releases initially travel to the south, then curve to the north and approach the release point from the northwest. Both schemes are represented by the black arrows in Fig. 10. Apparently, this is in contradiction with the known circulation patterns in the Arabian Sea (Schott and McCreary, 2001): anticyclonic in summer and cyclonic in winter. The point is that Fig. 10 is not a snapshot of winter/summer circulation. For instance, for

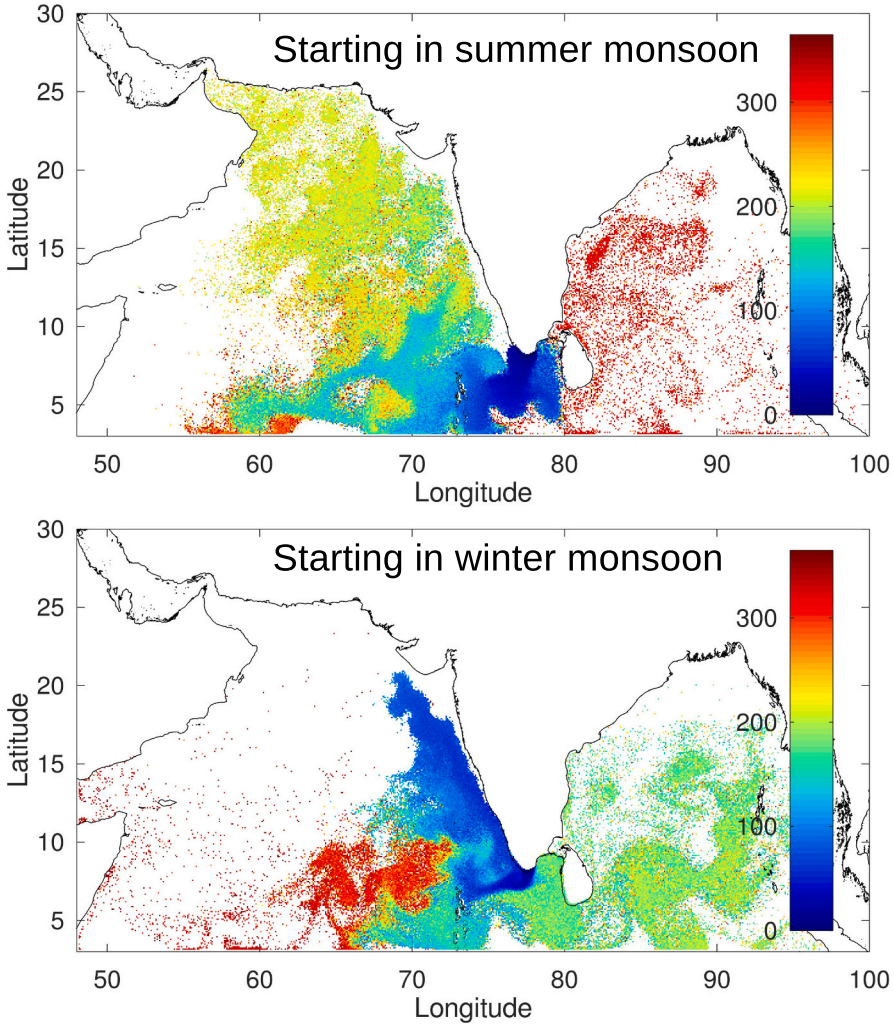

Fig. 11. Age distributions (days) in the surface layer for releases occurring from Kudankulam NPP starting on May 15th and December 15th (top and bottom respectively).

the winter simulation the radionuclide release is supposed to start in December 15th. Then, the release lasts for three months and nine additional months (without releases) are simulated. Thus, these maps represent an integration of circulation during a full year (with only 3 months of release). The final result is an *apparent* anticyclonic overall transport of the winter release, for instance, which at first sight contradicts the well-known Indian Ocean circulation scheme, correctly reproduced by HYCOM model (Fig. 3).

Results for the releases from Kudankulam NPP are presented in Fig. 11. Results of both simulations are now more different than in the case of Tarapur releases (Fig. 10) with respect to the extension of the radionuclide patch: the Arabian Sea is more affected by contamination if releases start in summer than if they start with the winter monsoon. The oscillatory nature of monsoon currents is clearly seen in these simulations. Thus, the oldest particles in the summer simulation (top of Fig. 11) are those introduced in the Bay of Bengal by the SMC, flowing to the east. However, currents are weaker in the Bay of Bengal than in the south of India (Fig. 3) and particles do not return to the release area when circulation reverses. In contrast, the oldest particles in the winter simulation are those of the western ocean, where they are introduced by the WMC. This can also be seen with the help of Fig. 9: winter releases from Kudankulam reach region 3 and 5 sooner than the summer releases. Most of these particles remain relatively close to the release area, between 65° to 70° longitude, where they are trapped in eddies.

Results for the releases from PFBR NPP may be seen in Fig. 12. As in the previous case, the Arabian Sea is more affected by radionuclides if the release starts with the summer monsoon. These releases seem to have been divided in two branches, since particles with similar ages are seen in the Arabian Sea and Bay of Bengal, far from the release point. Actually, these two branches are appreciated in the distribution of the younger particles in the top panel of Fig. 12. If the release starts with the winter monsoon, a significant number of particles are trapped in eddies around 70° E longitude (as in the case of Kudankulam), where the oldest particles are found. Again as in the previous case, it may be seen in Fig. 9 that releases starting in winter reach the western ocean sooner than releases starting in summer. As in the case of the Tarapur age distributions, these maps (Figs. 11 and 12) should not be interpreted as snapshots of radionuclide distributions.

4. Conclusions

A Lagrangian model which describes the transport of radionuclides in the northern Indian Ocean was described. The model includes physical transport (advection due to currents and mixing due to turbulence), interactions of radionuclides with bed sediments and radioactive decay. Water circulation was obtained from the well-known HYCOM ocean model. Three different mixing models were tested: the simplest one (constant and uniform horizontal and vertical diffusivities) provides a very fast response and a conservative estimation of concentrations in the release area, thus it may be useful if a rapid assessment after an accident

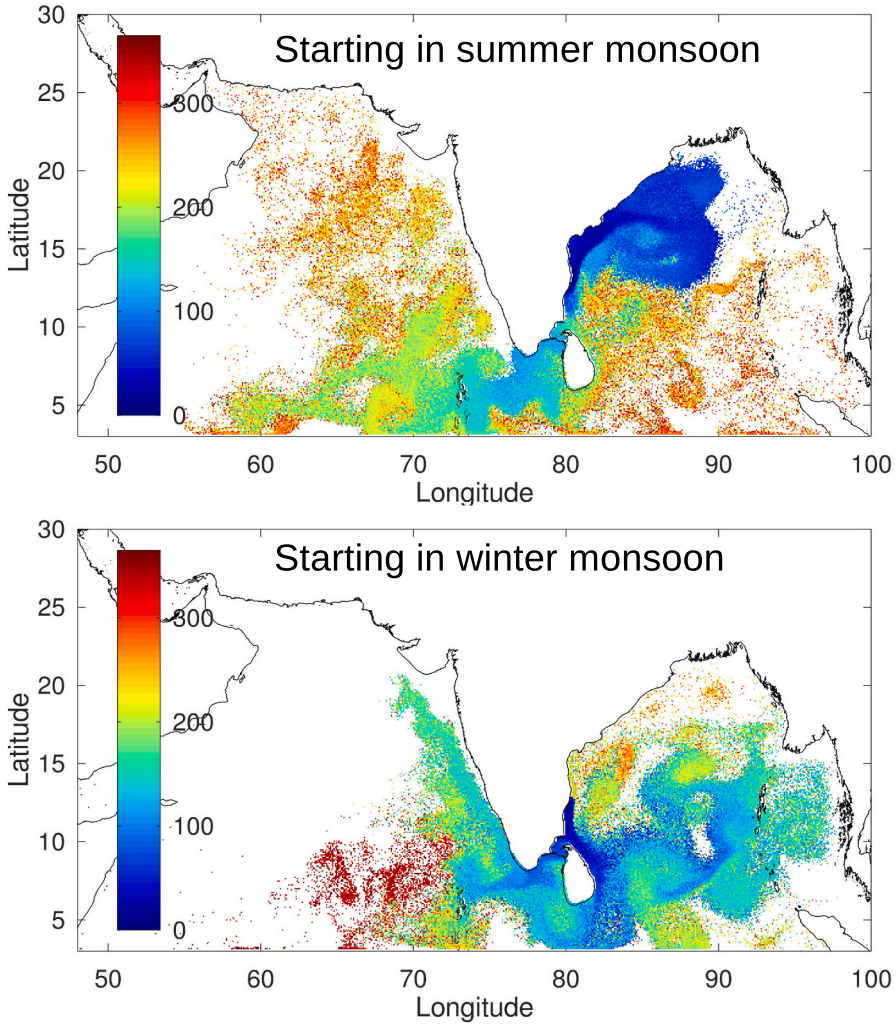

Fig. 12. Age distributions (days) in the surface layer for releases occurring from PFBR NPP starting on May 15th and December 15th (top and bottom respectively).

is required. More complex descriptions (Smagorinsky scheme for horizontal and variable vertical diffusivities) may be used for more refined calculations.

Hypothetical accidents occurring in NPPs located along the ocean coasts were simulated; they were supposed to occur both during the winter and summer monsoons. Seasonal differences were not as large as could initially be expected for the NPPs located in the Arabian Sea coast. In contrast, the major seasonal differences occur for the NPP located in the south of India, markedly influenced by the WMC and SMC.

. Also, the radionuclide distributions in the surface layer and in deep water were similar, although most of the released radionuclides are introduced into the deep ocean. The contamination of the bed sediments was found to be limited to the continental shelf.

Effective half-life of ^{137}Cs in the ocean surface was calculated, resulting about two orders of magnitude smaller than previous estimations carried out from measurements. This difference was attributed to the fact that external sources of radionuclides were not considered in such estimations and, also, to the small number of used measurements and their extrapolation from a local area to be considered as representative values for the whole ocean.

Age distributions of releases from the NPPs were calculated attaching a clock to each particle. Ages help to visualize transport patterns in the ocean; for instance releases in the western ocean tend to follow a cyclonic path if they occur in summer, but such pattern changes to anticyclonic in the case of winter releases.

The present model, as a summary, is a useful tool which could be applied to both the assessment of the consequences of a nuclear accident in a coastal NPP and also to more basic oceanographic research.

CRediT authorship contribution statement

R. Periáñez: conceptualization, methodology, formal analysis, writing (original draft)
B.I. Min: conceptualization, formal analysis, writing (review)
K.S. Suh: conceptualization, formal analysis, writing (review).

Declaration of competing interest

The authors declare that they have no known competing financial interests or personal relationships that could have appeared to influence the work reported in this paper.

Acknowledgement

This work was partially supported by the National Research Foundation of Korea (NRF) and funded by the Korean Government (MSIT): NRF-2017M2A8A4015253, NRF-2015M2A2B2034282, NRF-2020M2C9A1061641, as well as by Spanish Ministerio de Ciencia, Innovación y Universidades project PGC2018-094546-B-I00 and Junta de Andalucía (Consejería de Economía y Conocimiento) project US-1263369.

References

Bleck, R., 2001. An oceanic general circulation model framed in hybrid isopycnic-Cartesian coordinates. Ocean Model 4, 55–88.

Brovchenko, I., Maderich, V., 2021. Modelling radionuclide scavenging in the ocean by particle tracking in multicomponent medium with first-order reaction kinetics. In: Palagin, A., Anisimov, A., Morozov, A., Shkarlet, S. (Eds.), Mathematical Modeling and Simulation of Systems. MODS 2020. Advances in Intelligent Systems and Computing. Springer, pp. 36–46.

Collins, C., Hermes, J.C., 2019. Modelling the accumulation and transport of floating marine micro-plastics around South Africa. Mar. Pollut. Bull. 139, 46–58.

Cummings, J.A., 2005. Operational multivariate ocean data assimilation. Q. J. R. Meteorol. Soc. C 131 (613), 3583–3604.

Cummings, J.A., Smedstad, O.M., 2013. Variational data assimilation for the global ocean. In: Park, S., Xu, L. (Eds.), Data Assimilation for Atmospheric, Oceanic and Hydrologic Applications, vol. II. Springer, Berlin, Heidelberg, pp. 303–343.

Cushman-Roisin, B., Beckers, J.M., 2011. Introduction to Geophysical Fluid Dynamics. Elsevier.

Davies, A.M., Jones, J.E., Xing, J., 1997a. Review of recent developments in tidal hydrodynamic modeling. I: spectral models. J. Hydraul. Eng. 123, 278–292.

Davies, A.M., Jones, J.E., Xing, J., 1997b. Review of recent developments in tidal hydrodynamic modeling. II: turbulence energy models. J. Hydraul. Eng. 123, 293–302.

Deleersnijder, E., Capin, J.M., Delhez, E.J.M., 2001. The concept of age in marine modelling 1: theory and preliminary model results. J. Mar. Syst. 28, 229–267.

Elliott, A.J., Clarke, S., 1998. Shallow water tides in the Firth of Forth. Hydrogr. J. 87, 19–24.

Elliott, A.J., Wilkins, B.T., Mansfield, P., 2001. On the disposal of contaminated milk in coastal waters. Mar. Pollut. Bull. 42, 927–934.

IAEA, 2001. Generic models for use in assessing the impact of discharges of radioactive substances to the environment. In: Safety Reports Series, vol. 19 (Vienna).

IAEA, 2004. Sediment distribution coefficients and concentration factors for biota in the marine environment. In: Technical Reports Series, vol. 422 (Vienna).

IAEA, 2019. Modelling of Marine Dispersion and Transfer of Radionuclides Accidentally Released From Land Based Facilities. IAEA-TECDOC-1876 (Vienna).

Kobayashi, T., Nagai, H., Chino, M., Kawamura, H., 2013. Source term estimation of atmospheric release due to the Fukushima Dai-ichi Nuclear Power Plant accident by atmospheric and oceanic dispersion simulations. J. Nucl. Sci. Technol. 50, 255–264.

Nyffeler, U.P., Li, Y.H., Santschi, P.H., 1984. A kinetic approach to describe trace element distribution between particles and solution in natural aquatic systems. Geochim. Cosmochim. Acta 48, 1513–1522.

Patgaonkar, R.S., Vethamony, P., Lokesh, K.S., Babu, M.T., 2012. Residence time of pollutants discharged in the Gulf of Kachchh, northwestern Arabian Sea. Mar. Pollut. Bull. 64, 1659–1666.

Periáñez, R., 2008. A modelling study on ^{137}Cs and ^{239,240}Pu behaviour in the Alborán Sea, western Mediterranean. J. Environ. Radioact. 99, 694–715.

Periáñez, R., 2020. Models for predicting the transport of radionuclides in the Red Sea. J. Environ. Radioact. https://doi.org/10.1016/j.jenvrad.2020.106396.

Periáñez, R., Elliott, A.J., 2002. A particle tracking method for simulating the dispersion of non conservative radionuclides in coastal waters. J. Environ. Radioact. 58, 13–33.

Periañez, R., Kyung, K.S., Byung, M., Casacuberta, N., Masque, P., 2013. Numerical modelling of the releases of ^{90}Sr from Fukushima to the ocean: an evaluation of the source term. Environ. Sci. Technol. 47, 12305–12313.

Periáñez, R., Bezhenar, R., Brovchenko, I., Duffa, C., Jung, K.T., Kobayashi, T., Lamego, F., Maderich, V., Min, B.I., Nies, H., Osvath, I., Outola, I., Psaltaki, M., Suh, K.S., de With, G., 2016. Modelling of marine radionuclide dispersion in IAEA MODARIA program: lessons learnt from the Baltic Sea and Fukushima scenarios. Sci. Total Environ. 569 (570), 594–602.

Periáñez, R., Bezhenar, R., Brovchenko, I., Duffa, C., Iosjpe, M., Jung, K.T., Kobayashi, T., Liptak, L., Little, A., Maderich, V., Min, B.I., Nies, H., Osvath, I., Suh, K.S., de With, G., 2019a. Marine radionuclide transport modelling: recent developments, problems and challenges. Environ. Model. Softw. 122, 104523.

Periáñez, R., Bezhenar, R., Brovchenko, I., Jung, K.T., Kamidara, Y., Kim, K.O., Kobayashi, T., Liptak, L., Maderich, V., Min, B.I., Suh, K.S., 2019b. Fukushima ^{137}Cs releases dispersion modelling over the Pacific Ocean. Comparisons of models with water, sediment and biota data. J. Environ. Radioact. 198, 50–63.

Povinec, P., Aarkrog, A., Buesseler, K.O., Delfanti, R., Hirose, K., Hong, G.H., Ito, T., Livingston, H.D., Nies, H., Noshkin, V.E., Shima, S., Togawa, O., 2005. ^{90}Sr, ^{137}Cs and ^{239,240}Pu concentration surface water time series in the Pacific and Indian Oceans - WOMARS results. J. Environ. Radioact. 81, 63–87.

Proctor, R., Flather, R.A., Elliott, A.J., 1994. Modelling tides and surface drift in the Arabian Gulf: application to the Gulf oil spill. Cont. Shelf Res. 14, 531–545.

Proehl, J.A., Lynch, D.R., McGuillicuddy, D.J., Ledwell, J.R., 2005. Modeling turbulent dispersion on the North Flank of Georges Bank using Lagrangian particle methods. Cont. Shelf Res. 25, 875–900.

Sartandel, S.J., Jha, S.K., Tripathi, R.M., 2015. Latitudinal variation and residence time of ^{137}Cs in Indian coastal environment. Mar. Pollut. Bull. 100, 489–494.

Schiller, A., Oke, P.R., 2015. Dynamics of ocean surface mixed layer variability in the Indian Ocean. J. Geophys. Res. Oceans 120, 4162–4186.

Schott, F.A., McCreary, J.P., 2001. The monsoon circulation of the Indian Ocean. Prog. Oceanogr. 51, 1–123.

Shankar, C., Vinayachandran, P.N., Unnikrishnan, A.S., 2002. The monsoon currents in the North Indian Ocean. Prog. Oceanogr. 52, 63–120.

Suneel, V., Vethamony, P., Kumar, K.V., Babu, M.T., Prasad, K.V.S.R., 2013. Simulation of trajectories of tar ball transport to the Goa Coast. Water Air Soil Pollut. 224, 1538.

Tomczak, M., Godfrey, J.S., 2003. Regional Oceanography: An Introduction. Daya Publishing House, Delhi.

Zhang, L., Yan, Du, Cai, Wenju, 2018. A spurious positive Indian Ocean Dipole in 2017. Sci. Bull. 63 (18), 1170–1172.

Zhang, L.Y., Du, Y., Cai, W., Chen, Z., Tozuka, T., Yu, J.Y., 2020. Triggering the Indian Ocean Dipole from the Southern Hemisphere. Geophysical Research Letters, 47, e2020GL088648.